Morphology and structure of diamond-like carbon film induced by picosecond laser ablation

Keisuke Takabayashi*1, Takashi Takahashi*2, Eibon Tsuchiya*2, Kazuki Mimura*3, Yoshiyuki Yamamoto*1, Yohei Kobayashi*2, Takuro Tomita*3, Makoto Yamaguchi*1

*1:Akita University, *2: Institute for Solid State Physics, The University of Tokyo, *3:Tokushima University

Abstract

Raman spectroscopy was performed to investigate the laser-induced microscopic structural changes in diamond-like carbon known as tetrahedral amorphous carbon. Coarse laser-induced periodic surface structures (LIPSSs) at the center of the crater and fine LIPSSs at the upper and lower peripheral regions of the

ablated crater were formed via laser irradiation. An analysis of the Raman spectra via mapping measurements around the periphery of the crater demonstrated an increase in defect density occurred without morphological or structural changes. In irradiated areas with a higher local fluence, clustering and crystallization of sp^2 occurred. The relationship between the crystalline structural changes and the local fluence was discussed.

Keywords: Raman spectroscopy, ps laser, DLC, LIPSS

Introduction

Laser-matter interactions have been receiving significant interest. In solid materials, intense laser irradiation causes irreversible morphological and/or structural changes such as material processing and improved material properties. The use of ultrashort pulse lasers with pulse durations of the order of picoseconds (ps) to femtoseconds (fs) can realize unique and interesting phenomena, such as a low thermal effect and an extremely small modification size, which provide several advantages compared with a continuous wave or nanosecond laser irradiation [1-3].

Laser-induced periodic surface structures (LIPSSs), called ripples, can be spontaneously produced after laser irradiation. The morphology depends on the incident beam parameters, such as laser polarization, fluence, and the accumulated number of pulses [4-8]. LIPSSs are classified as coarse or fine according to their spatial period. Coarse LIPSSs, which have a spatial period similar to the wavelength of the incident laser, have been reported for various pulse durations and target materials. Using an fs laser, fine LIPSSs, which have a period equal to 1/3–1/10 times that of the incident laser, have been reported for silicon and diamond-like carbon (DLC). The formation mechanism has been extensively discussed in the literature [9].

Although numerous studies have reported laser-induced morphologies on solid surfaces such as LIPSSs, few studies have discussed the microscopic properties of the laser-induced material phase. During the formation of fine LIPSSs on DLC, which is an amorphous material, the surface layer is changed to nanocrystalline graphite [8]. During the formation of LIPSSs on crystalline silicon, which is a single atomic system, polymorph silicon and an amorphous phase of silicon (a-Si) have been observed [10]. For fine and coarse LIPSSs on silicon carbide (SiC), which is a two-atomic system, amorphous phases of SiC

(a-SiC) and a-Si, and an amorphous phase of carbon were observed; a-SiC was observed only on fine LIPSSs [11, 12]. The degree of crystallinity is disturbed on fine LIPSSs, and the subsequent separation of silicon and carbon atoms occurs on coarse LIPSSs. Studies on the microscopic structure reveal laser-induced modifications, including the mechanisms of LIPSS formation.

In this paper, we present the laser-induced morphology and microscopic structure of DLC coatings. Because carbon-based materials would undergo many structural changes, DLC, which is an amorphous material in an unstable state, was used as the test sample. The morphology was examined via atomic force microscopy (AFM) and field-emission scanning electron microscopy (FE-SEM). Micro-Raman spectroscopy, which is a nondestructive and noncontact method for characterizing the bonding structure of a sample, was used to characterize the structural changes. Raman spectroscopy is widely used to characterize carbon-based materials because it is strongly influenced by their crystalline structure and bond disorder. A spatial distribution, that is, the local fluence dependence of the structural change, was obtained via mapping measurements.

Materials and methods

Tetrahedral amorphous carbon (ta-C) is a hydrogen-free DLC material with a high proportion of sp^3 bonds. The film was deposited on a silicon substrate with a thickness of approximately 100 nm. The sample was irradiated using a Yb-doped fiber laser with a wavelength of 1.03 μm, repetition rate of 1 MHz, and pulse duration of 3.1 ps. The accumulated number of pulses was 10^5, which was controlled by changing the exposure time of the mechanical shutter. The intensity profile of the laser spot was an elliptical Gaussian profile with long and short axes ($1/e^2$) of approximately 6.4 μm and 4.2 μm, respectively. The values were estimated using a CMOS camera (Camera Module 2 NoIR, Raspberry Pi Foundation). The laser power was adjusted using a setup comprising a half-wave plate and polarized beam splitter. The peak fluence was approximately 0.2 J/cm^2. Laser irradiation was performed at room temperature under atmospheric conditions.

The sample surface was inspected using FE-SEM (Hitachi, S-4700) and AFM (JEOL Ltd., JSPM-5200). AFM was used to characterize the laser-induced morphology of the sample so the cross-sectional profile could be examined. A silicon cantilever with a resonance frequency of approximately 280 kHz was used

under ambient conditions. Micro-Raman spectroscopy was performed at room temperature (Horiba, LabRam HR Evolution) to characterize the laser-induced structure of the sample. The excitation wavelength was set to 355 nm. The wavenumbers were calibrated using the Raman shift of the first-order phonon peak of the single-crystal Si. The wavenumber resolution was approximately 4 cm^{-1}. A 40x objective lens was used, and the diameter of the laser spot was approximately 1 μm. Therefore, the spatial resolution was estimated to be 1 μm. The mapping measurement was performed with a resolution of 0.25 μm and 0.5 μm in lateral and vertical directions, respectively, to characterize the spatial distribution of laser-induced structural change, which correlates with the local fluence.

Results and discussion

Morphological changes on the DLC surface were induced by laser irradiation. Figure 1 shows an SEM image of a laser-irradiated crater. An elliptical crater corresponding to the intensity profile of the incident laser beam and fine LIPSSs at the upper and lower edges of the crater were observed.

Figure 2 (a) shows the topographical AFM image. The crater profile was elliptic and approximately 4.4 μm and 2.3 μm in lateral and vertical directions, respectively. The fine LIPSSs have a mean spatial period of approximately 330 nm. Figure 2 (b) shows the cross-sectional profile of the laser crater along the white dashed line that runs through the center of the crater in Fig. 2 (a). The horizontal axis in Fig. 2(b) was set to 0 μm, and the crater depths were approximately 29 nm and 58 nm at 0 μm and 0.8 μm, respectively. Fig. 2(b) also shows coarse LIPSSs with a spatial period of approximately 1.2 μm and an amplitude of approximately 14 nm.

Figure 3 shows Raman spectra measured on the unirradiated area and center of the crater. Spectra are normalized to the intensity of approximately 520 cm^{-1}. Because the excitation light was penetrating substrate silicon, the first- and second-order transverse optical (TO) phonon peaks of silicon can be observed at approximately 520 and 1000 cm^{-1}, respectively [13]. Peaks at 1600 cm^{-1}, which can be attributed to DLC film, are also visible. [14] The spectral shape around the peak is due to the DLC at the center of the crater having changed compared to the unirradiated area. This indicates a structural change in the DLC.

As previously reported, amorphization, poly-crystallization [5, 15], and nano-crystallization of silicon [16] by laser irradiation affect the peak around 480 cm^{-1} [17], the asymmetry of the TO phonon of silicon, and the peak of photoluminescence [18] in the spectrum, respectively. In this study, no significant changes were observed in the spectra of silicon. The ablation threshold was reported as 0.22 J/cm^2 [19], which is higher than that of the DLC. Therefore, we conclude that the silicon substrate was not affected by laser irradiation.

A regression analysis was performed to determine the spectral shape. The Levenberg–Marquardt algorithm was used for the analysis (R language, minpack library). An example of fitting the Raman spectrum at the crater center is shown in Fig. 4. In Fig. 4, curve (a) shows a typical Raman spectrum at the crater center, and curve (b) shows the fitting results for curve (a) and curves (c)–(f) show the fitting elements used for curve (b). The Raman spectrum of the DLC film has D and G peaks due to the defects and sp^2 bonds of carbon, respectively [14]. The fitting function for the DLC was composed of D, G, and two additional peaks. The Lorentzian function for the D peak, the pseudo-Voigt function, which is a combination of Gaussian and Lorentzian functions for the G

peak, and two Gaussian functions for additional DLC peaks around 1100 cm^{-1} and 1400 cm^{-1} were used. Note that the pseudo-Voigt function used for the G peak has independent parameters on the left and right sides and is asymmetric. The fitting functions for the second-order phonons of silicon are a combination of Gaussian and Lorentzian functions; a linear function was used as the baseline.

Figures 5 (a), (b), and (c) show the relationship between the center wavenumber of the G peak (ω_G), relative intensity of the D peak to the G peak (I_D/I_G), half width at half maximum for the high wavenumber side of the G peak ($HWHM_G$), and local fluence that follows the laser spot profile of the laser pulse. The laser spot was approximated as the product of two Gaussian functions with the widths and peak fluence outlined in the Methods section. The local fluence value at each point was determined using Gaussian approximation with a peak fluence of 0.2 J/cm^2 and the distance from the center. Note that the mapping position of the Raman spectroscopy was calibrated, and the spatial distribution of I_D/I_G was symmetrical. As the local fluence increased, ω_G and $HWHM_G$ decreased and I_D/I_G increased. The thresholds for change of ω_G, I_D/I_G, and $HWHM_G$ are approximately 0.12 J/cm^2, 0.14 J/cm^2, and 0.14 J/cm^2, respectively. Corresponding to the AFM image of the local fluence, fine LIPSS was observed

in part of the local fluence from 0.14 J/cm^2 to 0.16 J/cm^2. At this local fluence range, no significant difference was observed between the crystalline structures where fine LIPSS was formed and not formed. The threshold fluences for crater formation and fine LIPSS formation were obtained, with values of 0.16 J/cm^2 and 0.14 J/cm^2, respectively. The thresholds for the Raman spectral shape and morphological changes were nearly identical.

Figure 6(a) shows the relationship between I_D/I_G and HWHM$_G$, where the local fluence is less than 0.10 J/cm^2 and the values of I_D/I_G and HWHM$_G$ are approximately 0.17 cm^{-1} and 110 cm^{-1}, respectively. The relationship between I_D/I_G and HWHM$_G$ varies linearly from the upper left to the lower right in the figure. This implies that I_D/I_G and HWHM$_G$ change in correlation with an increase in local fluence. Figure 6(b) shows the relationship between I_D/I_G and ω_G, where a local fluence is less than 0.10 J/cm^2 and the value of ω_G is approximately 1598 cm^{-1}. Although I_D/I_G is almost similar at approximately 0.17 cm^{-1}, which corresponds to the value in the unirradiated area, a large shift in ω_G to a low wavenumber can be observed. This implies that the shift in ω_G occurs at a lower fluence than the spectral changes.

A schematic of the laser-induced structure is shown in Fig. 7. An increase in I_D/I_G and a decrease in ω_G Raman spectra of DLC have been reported, resulting in the clustering of the sp^2 phase and an increase in bond disorder, respectively [20]; the decrease in $HWHM_G$ suggests sp^2 crystallization. Considering this, the current experimental results indicate that the defects in the DLC increased at the initial stage of laser-induced modification at the threshold fluence of approximately 0.12 J/cm^2, as shown in Fig. 5 (a). With increasing laser fluence, at approximately 0.14 J/cm^2, as shown in Figs. 5 (b) and (c), clustering and crystallization of the sp^2 bond occurred. This structural change suggests that an amorphous (ta-C) to sp^2 transition occurred, and the sp^2 components gathered to form clusters. Fine LIPSSs were also formed, associated with the morphological change at a fluence of approximately 0.14 J/cm^2–0.16 J/cm^2. Finally, at a fluence of 0.16 J/cm^2, a laser-induced crater and coarse LIPSSs were formed at the bottom of the crater.

Conclusion

In this paper, we reported the morphological and structural changes in a tetrahedral amorphous carbon film (DLC) deposited on silicon using an

ultrashort laser with a wavelength of 1.03 μm and pulse duration of 3.1 ps. The laser spot observed on the sample surface was an elliptical Gaussian profile, which had a radius ($1/e^2$) of approximately 6.4 μm and 4.2 μm in horizontal and lateral directions, respectively.

On the sample surface, an elliptical laser crater corresponding to the beam profile, with coarse LIPSSs in the center of the crater and fine LIPSSs at the upper and lower edges of the irradiation crater, was observed. The threshold fluences for the craters with coarse and fine LIPSS formation were 0.16 J/cm^2 and 0.14 J/cm^2, respectively.

Micro-Raman spectroscopy via mapping measurements was performed, and the threshold fluence for structural changes was investigated based on the spatial distribution of the bonding structure. A decrease in ω_G and $HWHM_G$ and an increase in I_D/I_G were observed. The threshold fluence for peak shift was approximately 0.12 J/cm^2. The threshold fluence for the increase in I_D/I_G and the sharpening of the G peak was 0.14 J/cm^2. At a fluence of approximately 0.12 J/cm^2, the number of defects increased during the initial stage of laser-induced modification.

As the fluence increased to approximately 0.14 J/cm^2, fine LIPSSs were formed on the morphology, with clustering and sp^2 crystallization occurring in the Raman spectrum. This suggests that an amorphous (ta-C) to sp^2 transition occurred and the sp^2 components gathered to form clusters.

Acknowledgments

This study was conducted at the Institute for Solid State Physics, University of Tokyo. It was supported by the AMADA FOUNDATION.

References

[1] D. von der Linde, K. Sokolowski-Tinten, Appl. Surf. Sci., The physical mechanisms of short-pulse laser ablation. 154–155, 1–10 (2000). https://doi.org/10.1016/S0169-4332(99)00440-7

[2] B. N. Chichkov, C. Momma, S. Nolte, F. Y. Alvensleben, A. Tünnermann, Appl. Phys. A, Femtosecond, picosecond and nanosecond laser ablation of solids. 63, 109–115 (1996). https://doi.org/10.1007/BF01567637

[3] F. Korte, J. Serbin, J. Koch, A. Egbert, C. Fallnich, A. Ostendorf, B. N. Chichkov, Appl. Phys. A, Towards nanostructuring with femtosecond laser pulses. 77, 229–235 (2003). https://doi.org/10.1007/s00339-003-2110-z

[4] G. Miyaji, K. Miyazaki, Opt. Express, Origin of periodicity in nanostructuring on thin film surfaces ablated with femtosecond laser pulses. 16, 16265–16271 (2008). https://doi.org/10.1364/oe.16.016265

[5] J. Bonse, S. Baudach, J. Krüger, W. Kautek, M. Lenzner, Appl. Phys. A, Femtosecond laser ablation of silicon–modification thresholds and morphology. 74, 19–25 (2002). https://doi.org/10.1007/s003390100893

[6] J. Bonse, J. Krüger, S. Höhm, A. Rosenfeld, J. Laser Appl., Femtosecond laser-induced periodic surface structures. 24, 4 (2012). https://doi.org/10.2351/1.4712658

[7] N. Yasumarua, H. Kasashima, E. Sentoku, H. Funabora, R. Tominaga, T. Harigai, H. Takikawa, Diam. Rela Mat., Corrosion performance of DLC coatings with laser-induced graphitized periodic surface structure. 109. https://doi.org/10.8046(2020)

[8] N. Yasumaru, E. Sentokua, T. Toya, R. Tominaga, T. Harigai, H. Takikawa, T. Tanimoto, Diam. Rela Mat., Laser-induced graphitized periodic surface structure formed on tetrahedral amorphous carbon films. 107. https://doi.org/10.7909(2020)

[9] K. Miyazaki, G. Miyaji, Appl. Phys. A, Mechanism and control of periodic surface nanostructure formation with femtosecond laser pulses. 114, 177–185 (2014). https://doi.org/10.1007/s00339-013-8130-4

[10] F. Costache, S. K. Kouteva-Arguirova, J. Reif, Appl. Phys. A, Sub-damage-threshold femtosecond laser ablation from crystalline Si: Surface nanostructures and phase transformation. 79, 1429–1432 (2004). https://doi.org/10.1007/s00339-004-2803-y

[11] M. Yamaguchi, S. Ueno, R. Kumai, K. Kinoshita, T. Murai, T. Tomita, S. Matsuo, S. Hashimoto, Appl. Phys. A, Raman spectroscopic study of femtosecond laser-induced phase transformation associated with ripple

formation on single-crystal SiC. 99, 23–27 (2010).

https://doi.org/10.1007/s00339-010-5569-4

[12] T. Tomita, T. Okada, H. Kawahara, R. Kumai, S. Matsuo, S. Hashimoto, M. Kawamoto, M. Yamaguchi, S. Ueno, E. Shindou, A. Yoshida, Appl. Phys. A, Microscopic analysis of carbon phases induced by femtosecond laser irradiation on single-crystal SiC. 100, 113–117 (2010). https://doi.org/10.1007/s00339-010-5786-x

[13] P. Mishra, K. P. Jain, Phys. Rev. B, First- and second-order Raman scattering in nanocrystalline silicon. 64, 073304 (2001).

https://doi.org/10.1103/PhysRevB.64.073304

[14] A. C. Ferrari, J. Robertson, Philos. Trans. A Math. Phys. Eng. Sci., Raman spectroscopy of amorphous, nanostructured, diamond-like carbon, and nanodiamond. 362, 2477–2512 (2004). https://doi.org/10.1098/rsta.2004.1452

[15] J. Bonse, K.-W. Brzezinka, A. J. Meixner, Appl. Surf. Sci., Modifying single-crystalline silicon by femtosecond laser pulses: An analysis by micro Raman

spectroscopy, scanning laser microscopy and atomic force microscopy. 221, 215–230 (2004). https://doi.org/10.1016/S0169-4332(03)00881-X

[16] L. Zhang, K. Chen, X. Huang, L. Wang, J. Xu, W. Li, Appl. Phys. A, Control of size and shape of nc-Si in a-SiNx/aSi:H multilayers by laser induced constrained crystallization. 77, 485–489 (2003). https://doi.org/10.1007/s00339-002-1473-x

[17] K. Wu, X. Q. Yan, M. W. Chen, Appl. Phys. Lett., In situ Raman characterization of reversible phase transition in stress-induced amorphous silicon. 91 (2007). https://doi.org/10.1063/1.2779933

[18] B. Ghosh, N. Shirahata, influence of oxidation on temperature-dependent photoluminescence properties of hydrogen-Terminated silicon nanocrystals, Crystals. 10, 143 (2020). https://doi.org/10.3390/cryst10030143

[19] T. Takahashi, S. Tani, R. Kuroda, Y. Kobayashi, Appl. Phys. A, Precision measurement of ablation thresholds with variable pulse duration laser. 126, 582 (2020). https://doi.org/10.1007/s00339-020-03754-5

[20] A. C. Ferrari, J. Robertson, Phys. Rev. B, Interpretation of Raman spectra of disordered and amorphous carbon. 61, 20 (2000).

https://doi.org/10.1103/PhysRevB.61.14095

Captions

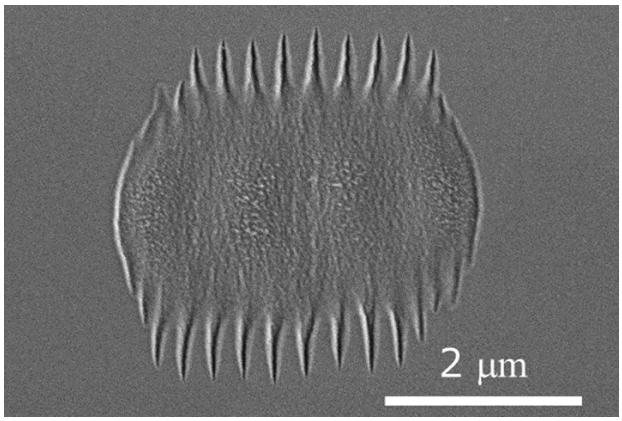

Fig. 1 SEM image of a laser-induced morphology. An elliptical crater that corresponds to the beam profile in the center and fine LIPSSs at the upper and lower edges of the crater are visible.

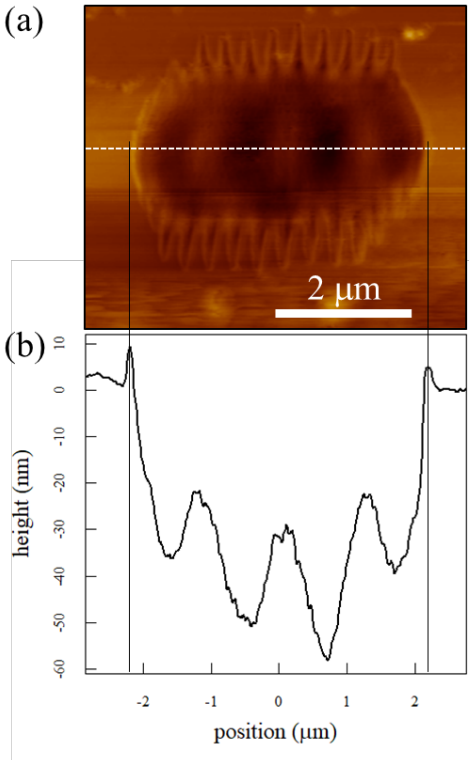

Fig. 2 (a) AFM topography image. (b) Cross-sectional profile of the laser crater along the dashed line in (a). The dashed line crosses the crater center.

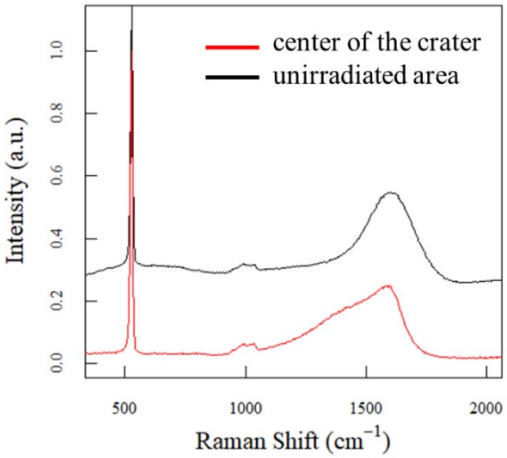

Fig. 3 Raman spectra measured on the unirradiated area (black) and the center of the crater (red). The ps laser beam was irradiated with a peak fluence of 0.2 J/cm^2 and pulse duration of 3.1 ps, and the accumulated number of pulses was 10^5. Peaks formed due to silicon and DLC can be observed.

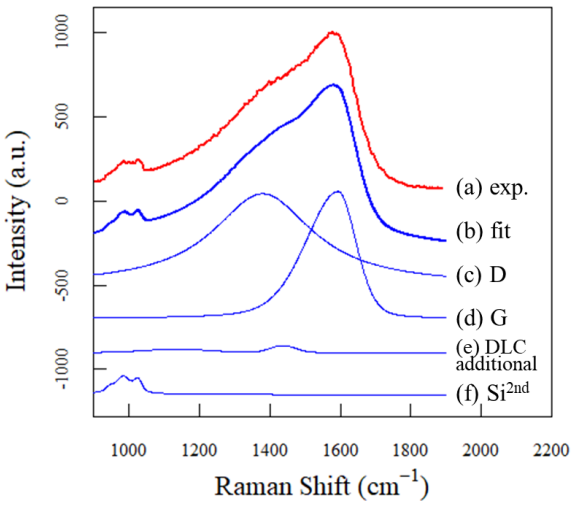

Fig. 4 Fitting results of the Raman spectrum at the crater center. Spectra are displayed with the decomposed elements.

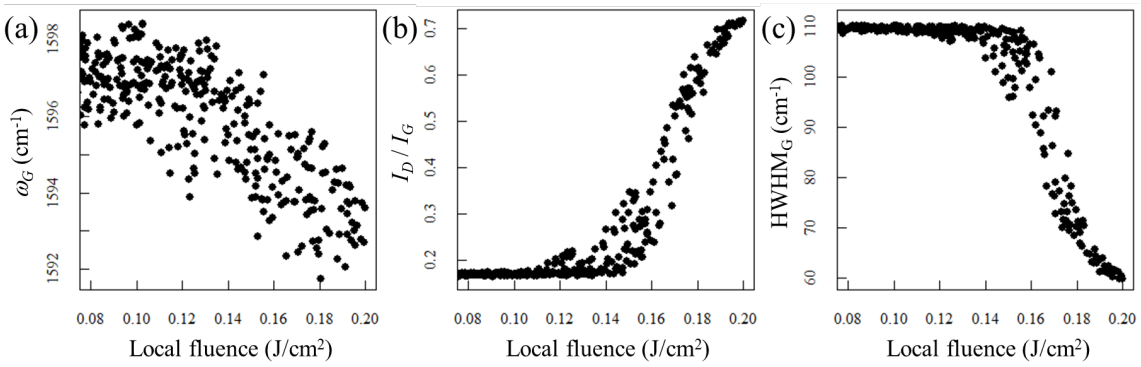

Fig. 5 Relationship with respect to local fluence of (a) center wavenumber of G peak (ω_G), (b) relative intensity of D peak to G peak (I_D/I_G), and (c) half width at half maximum for high wavenumber side of G peak ($\mathrm{HWHM_G}$)

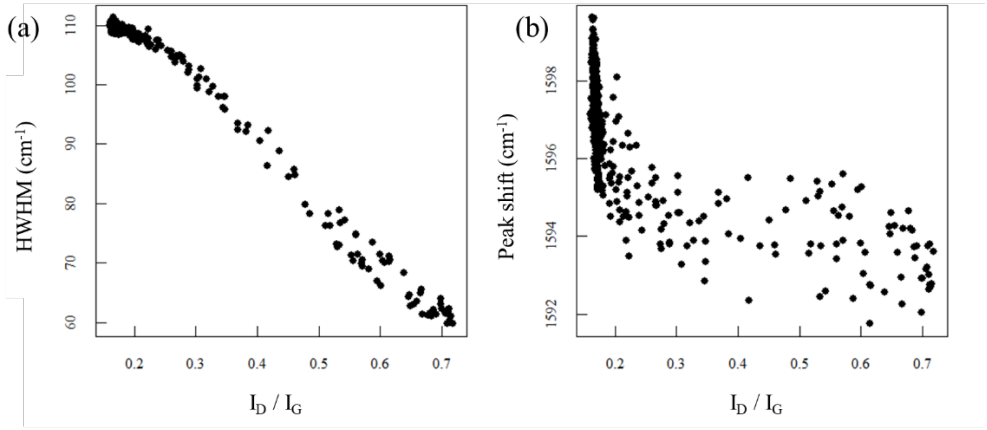

Fig. 6 Relationship between (a) relative intensity of D peak to G peak and HWHM for high wavenumber side of G peak and (b) relative intensity of D peak to G peak and a center wavenumber of G peak to local fluence

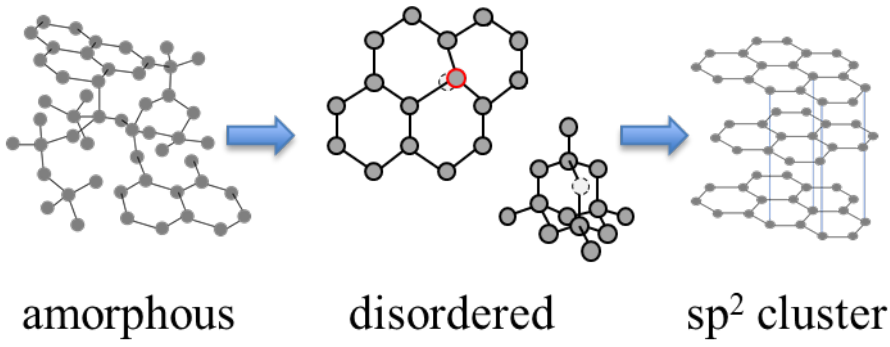

Fig. 7 Schematic of the laser-induced structure of non-irradiated DLC